NOAA Technical Memorandum ERL WPL-57

FM-CW RADAR OBSERVATIONS IN NORTHEASTERN COLORADO COMPARED WITH RAWINSONDE-MEASURED PROFILES OF REFRACTIVE INDEX

E. Gossard
R. Chadwick
D. Wolfe

Wave Propagation Laboratory
Boulder, Colorado
May 1980

noaa NATIONAL OCEANIC AND ATMOSPHERIC ADMINISTRATION / Environmental Research Laboratories

NOAA Technical Memorandum ERL WPL-57

FM-CW RADAR OBSERVATIONS IN NORTHEASTERN COLORADO COMPARED WITH RAWINSONDE-MEASURED PROFILES OF REFRACTIVE INDEX

E. Gossard
R. Chadwick
D. Wolfe

Wave Propagation Laboratory
Boulder, Colorado
May 1980

UNITED STATES
DEPARTMENT OF COMMERCE
Philip M. Klutznick, Secretary

NATIONAL OCEANIC AND
ATMOSPHERIC ADMINISTRATION
Richard A. Frank, Administrator

Environmental Research
Laboratories
Wilmot N. Hess, Director

CONTENTS

FM-CW RADAR OBSERVATIONS IN NORTHEASTERN COLORADO COMPARED WITH RAWINSONDE-MEASURED PROFILES OF REFRACTIVE INDEX

E. Gossard, R. Chadwick and D. Wolfe
NOAA/ERL/Wave Propagation Laboratory

ABSTRACT

This report deals primarily with a long period during which the FM-CW radar and a RAWINSONDE station were operated side-by-side in the NHRE program in 1974. The RAWINSONDE station and the FM-CW radar were colocated at Sterling in northeastern Colorado. Three balloons a day were launched while the radar operated in a vertically pointing, non-Doppler mode.

It is concluded that the radar is a reliable detector of elevated refractive layers. In fact it provides a better estimate of the height and persistency of such layers than do balloon soundings because layers undulate and the refractive index distribution is often transient and patchy. Single balloon sounding data cannot provide the important persistency information.

Insects are shown to be an important contaminant in the radar observations. It is demonstrated that insect targets are adequately separated from the clear-air returns if the range resolution of the radar is good (typically 3 m in the case of the Sterling observations). This ability is needed in biogeographical areas such as the U.S. Midwest if the clear-air elevated layers of meteorological interest are to be distinguished from insect layers.

1. INTRODUCTION

In this report radar backscatter from the optically clear air is compared with the meteorological structure as measured by RAWINSONDE. The radar used was a frequency-modulated, continuous-wave radar (Richter, 1969) with a Doppler capability to sense wind velocity (Strauch et. al, 1975: Chadwick et al., 1975). This report describes backscatter data acquired while the radar was operated for four weeks in a vertically pointing mode alongside a RAWINSONDE station that launched balloons 3 times a day at 07-08, 12-13, 15-16 MST. It is the longest continuous period of side-by-side data so far obtained. In addition, two well documented cases of frontal inversion layers recorded at Boulder, CO are included.

The strength of the backscattered signal from such a radar, pointing vertically, is clearly related to the turbulent structure and stratification of the atmosphere (Richter and Gossard, 1970). It is obviously desirable to establish this relationship as quantitatively as possible. Potential applications include the use of radar backscatter to improve the height resolution and accuracy of the radiometric retrieval of refractive index profiles and to sense remotely the presence of elevated refractive layers that may cause radio and radar ducting or excessive tropo-scatter capable of jeopardizing the performance of secure military systems. In this report radar observations are compared with balloon soundings taken at about the same time at Sterling, Colorado.

2. OBSERVATIONS

The radar observations were acquired in a vertically pointing mode and, in this report, only range vs backscattered power are considered. The radiosonde observations were a special series of soundings made during the National Hail Research Experiment in 1974 at Sterling in northeastern Colorado. We have plotted temperature, wind speed, wind direction and potential refractive index ϕ. The potential refractive index can be expressed in terms of the potential temperature θ and potential vapor pressure e_p as follows:

$$\phi = \frac{77.6}{\theta}\left(1000 + \frac{4810e_p}{\vartheta}\right) \qquad (1)$$

where $\theta = T(1000/p)^{0.286}$, $e_p = (1000/p)e$, T is temperature in Kelvin, e is vapor pressure in millibars and p is pressure in millibars. Potential refractive index is then related to the modified refractive index N = (n-1) x 10^6, where n is refractive index, by (see Appendix A).

$$\phi = e^{0.714}\left[N\, f(Z) + 71.95(Z/H)e^{-Z/H}\right] \qquad (2)$$

where $f(Z) \simeq 1 - 0.286\,\frac{Z}{H}$ ... and H is the local scale height of atmospheric density.

The quantity ϕ is of interest because, like potential temperature, it is a quantity that is conserved in air parcels that are undergoing adiabatic motion. Much of the dynamic and kinematic formulation for the transport of heat and moisture can therefore be applied directly to potential refractive index.

3. DISCUSSION

Insects

From the radar records it is immediately clear that insects are a major source of radar return at the time of year when these observations were made. Therefore, such biological targets are an important concern for many applications in the U.S. midwest. Insects in this area become airborne at temperatures above about 10°C (50°F).

Examples of radar return from insects are shown in Figs. 1, 2, 3 and 4. The observations in Figs. 1, 2 and 3 were acquired on the night of 19 July 1974. We have chosen this particular record from many others with comparable numbers of insects because of the interesting wave event on the nocturnal inversion displayed by the insects. The wave event displayed by the insects is very similar to that reported by Gossard and Richter

(1970) from clear-air returns and shows the same nonlinear wave shape. The balloon sounding was taken at 0655 Mountain Standard Time the following morning, and it is shown with the record in Fig. 3. The insect distribution in the early portion of the record suggests that the insect population, whose source is presumably the surface, is strongly confined to the surface layer by the strong thermal stratification; although there are insects above the surface layer, the relative numbers above the inversion become greater as the night progresses. There is in fact some suggestion in waves 4, 5 and 6 of Fig. 1 that the waves may play a role in entraining insects (or rather projecting them) into the region above the inversion. As the night progresses the insect population near the surface decreases, leaving a substantial elevated layer of insects apparently bearing little relation to the temperature profile revealed by the balloon sounding at 0655 MST (during lowest frame of Fig. 1). No attempt has been made to correct for the larger volume intercepted by the beam at greater heights nor to account for the fact that the side-by-side transmit and receive antennas used in this type of radar have beams that only partially intercept near the ground because of their spatial separation. The record summarized in these figures suggests that insects may produce elevated layers of radar return unrelated to the temperature-humidity structure at the time, and any radar without resolution good enough to resolve the individual insect point targets will not be reliable as a tool to aid radiometric retrieval in some geographical areas; they may, in fact, lead to mis-interpretation unless judgment is exercised. This was probably a major problem with the PHOENIX data when the FM-CW radar was not operating at high resolution.

Often the insect targets and clear-air return occur in the same record, as seen in Fig. 4. Human judgment can then distinguish the clear-air return at a height of 1400 meters from the discrete (and sometimes diffuse) return from the insects. But such a separation would be extremely difficult to automate.

Figure 4 shows an afternoon case in which insects dominate the return, although a clear-air return associated with the capping inversion seen in the balloon sounding appears at the upper edge of the insect layer. Superficially, this record looks much like the nighttime record of Fig. 1, but the scale in Fig. 1 is 0-750 m whereas that in Fig. 4 is 0-3000 m. In Fig. 4 the insects are being convectively mixed more-or-less uniformly through the whole depth of the

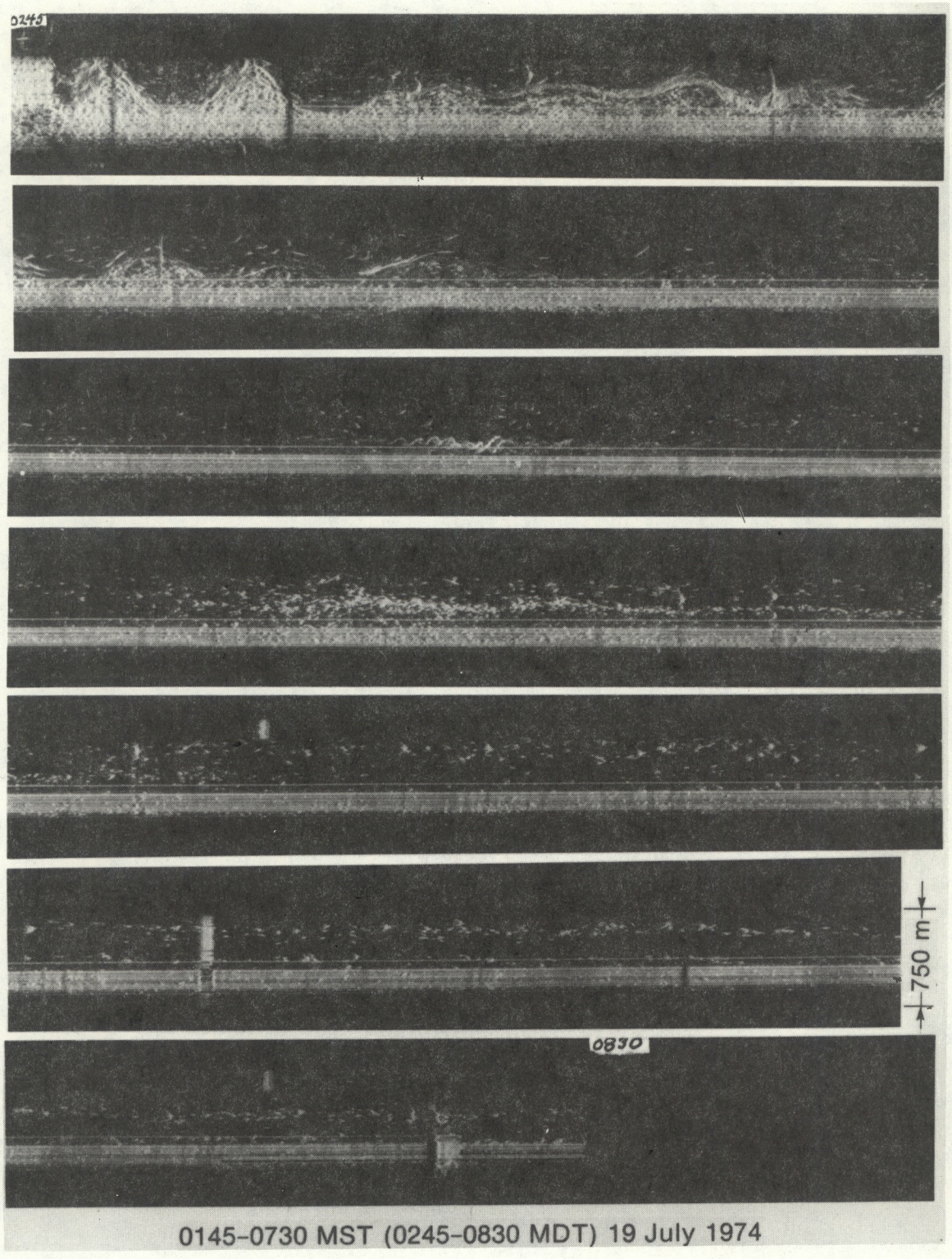

Figure 1. Example of point targets, that are probably insects, typical of many summer nights in the U.S. midwest. Note the non-linear gravity waves displayed by the insects near the beginning of the series. The trochoidal shape shows that the waves are very long compared with the layer depth (see Gossard and Richter, 1970). In the third frame from the top a series of Kelvin-Helmholtz shear instability features are seen, resembling breaking waves. Note elevated layer of insects that begins to form in frame 4 and the suggestion in the records that the insects are being entrained into the layer above the inversion at least partially by the wave motions. The resulting elevated layer of insects is not associated with a corresponding elevated layer in the temperature/humidity structure (see sounding in Fig. 3).

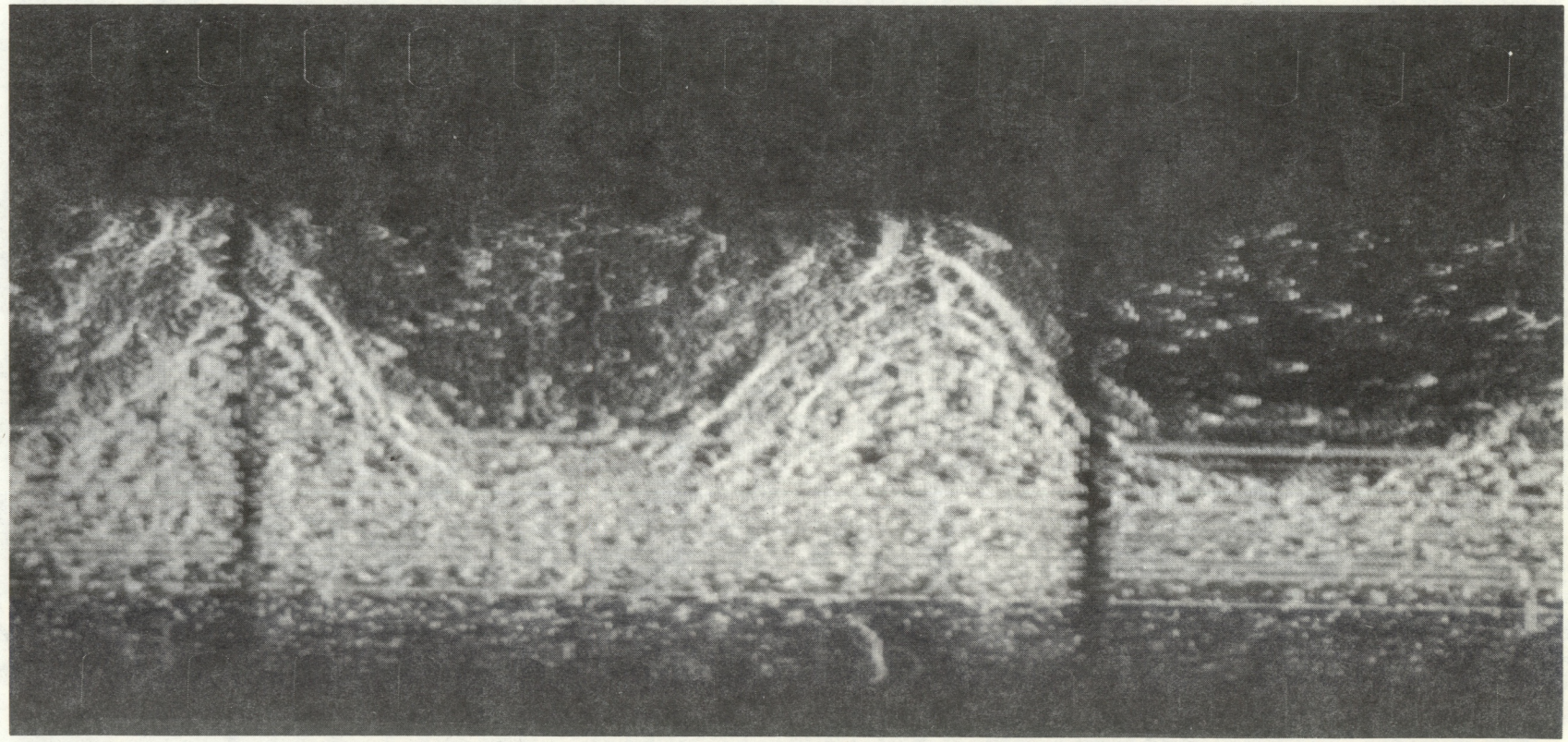

Figure 2. Detail of first few waves of Fig. 1. Wave period is 9 minutes.

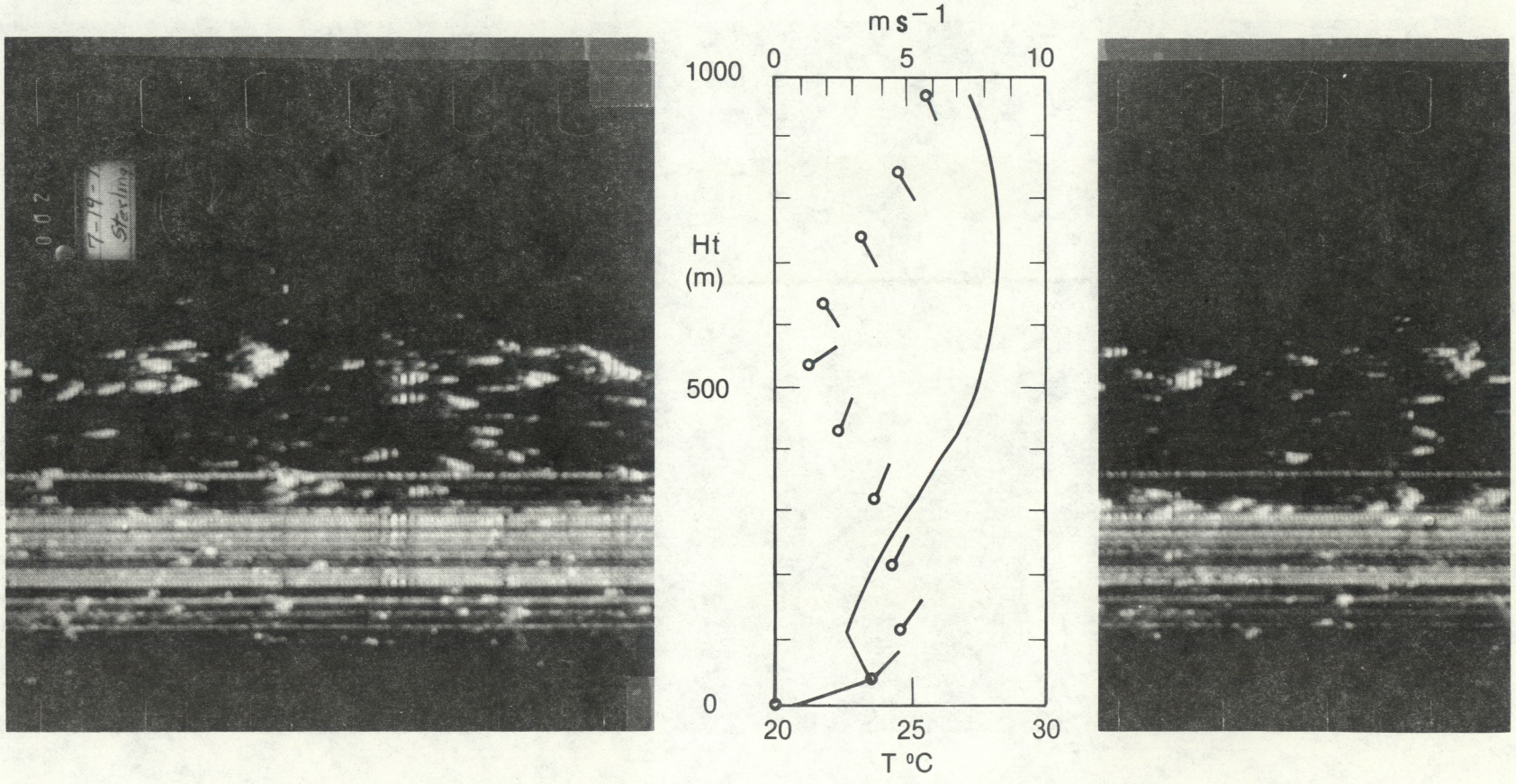

Figure 3. Detail of radar record near time of balloon sounding. Tail on velocity points (circles) indicates wind direction. For north wind tail is straight up.

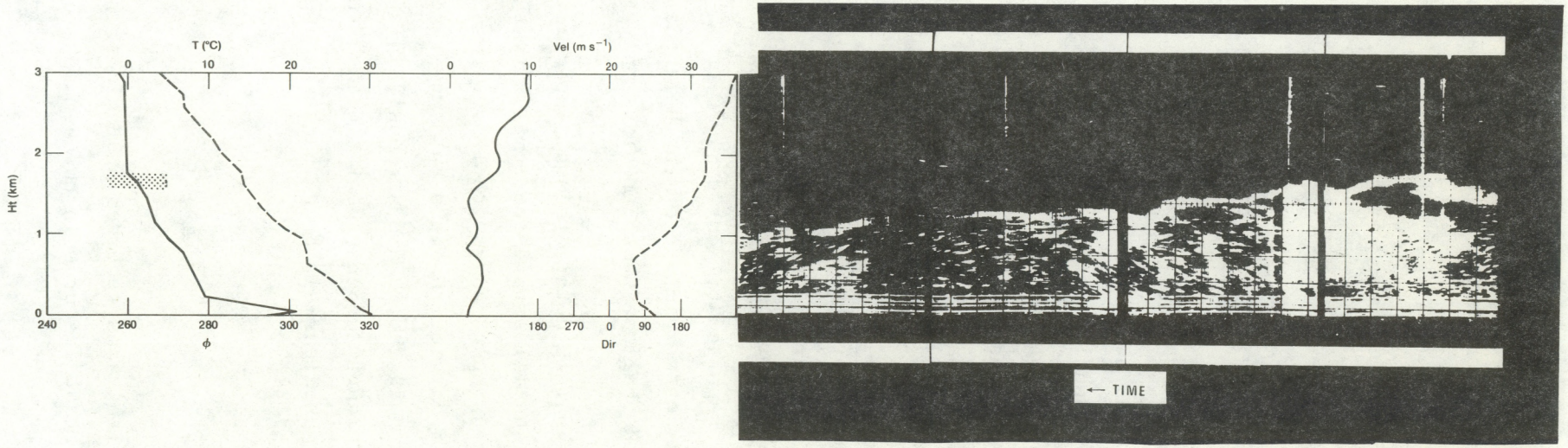

Figure 4. Record from 1229 - 1249 MST on afternoon of 14 June 1974 showing distribution of insects in daytime convection boundary layer. Raob release 1225 MST.

planetary boundary layer. It is perhaps significant that the insects reveal very little evidence of any entrainment through the capping inversion.

Convective Boundary Layer Capping Inversion

Figures 5, 6, 7, 8 and 9 show a clear relationship between the height of a layer of radar backscatter and a substantial negative gradient in potential refractive index.

Figure 11 is marginal. The radar record suggests a patch of clear-air return about 1/3 of the way through the record at a height that may correspond with the lower shaded layer on the sounding of ϕ. Toward the end of the record (left-hand side) a patch of clear-air return may represent the capping inversion shown as the upper shaded region on the sounding. Clearly the momentary structure of the time of balloon launch determines what the raob looks like in this case, and in this case the balloon probably passed between the regions containing layers.

Figure 10 shows examples of the convective domes so characteristic of the clear-air FM-CW radar returns previously described by Gossard et al. (1971) and Richter et al. (1974) and also seen in the Wallops Island records (in a quasi-horizontal pointing mode) reported by Konrad (1970). In these cases, it is clear that the radar provides a better picture of the height and variability of the capping layer than does the balloon which provides only an instantaneous "snap shot."

Figures 11 and 12 reveal in detail the way insects are swept up and entrained into convective features and illustrate the complexity that must characterize any analysis of such features using a radar with lesser resolution. The presence of insects contaminates the radar returns in such a way that predictions of wavelength dependence based on Bragg backscatter are seriously in error. Particulates such as insects produce a λ^{-4} wavelength dependence for backscattered power, if they are Rayleigh scatterers, whereas clear-air Bragg backscatter should have a dependence of about $\lambda^{-1/3}$.

Frontal Inversions

Figures 13-19 deal with cases recorded at Boulder, Colorado when frontal discontinuities were important features in the atmosphere above the radar. The

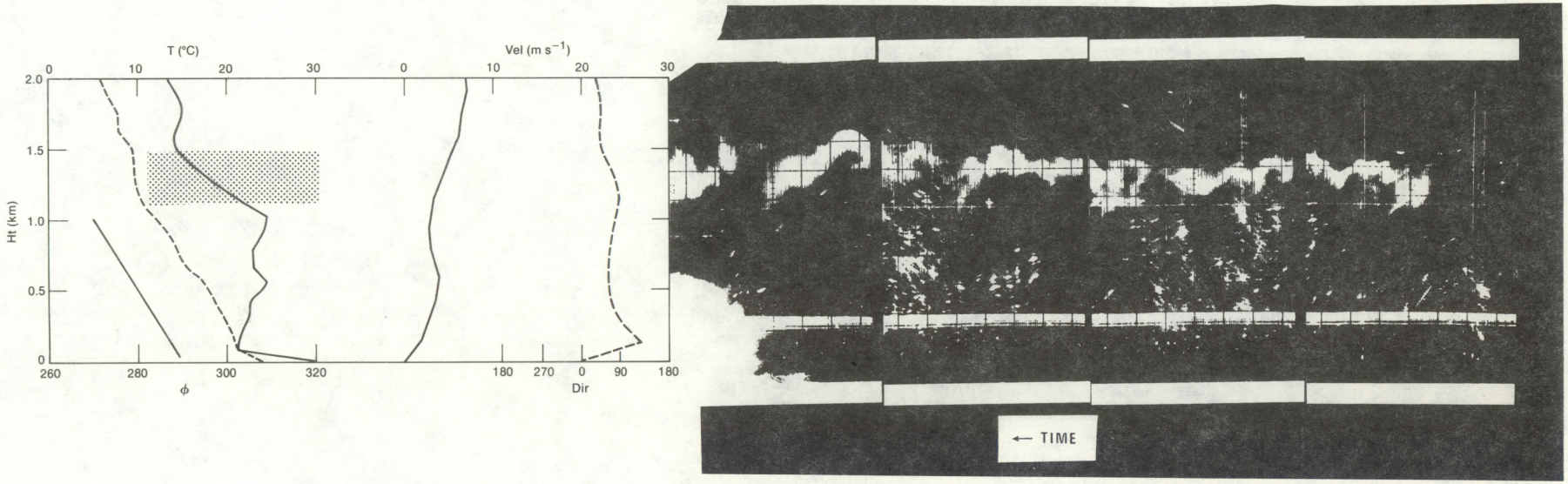

Figure 5. Record from 1206 - 1249 MST on 5 August 1974. Raob release 1225 MST.

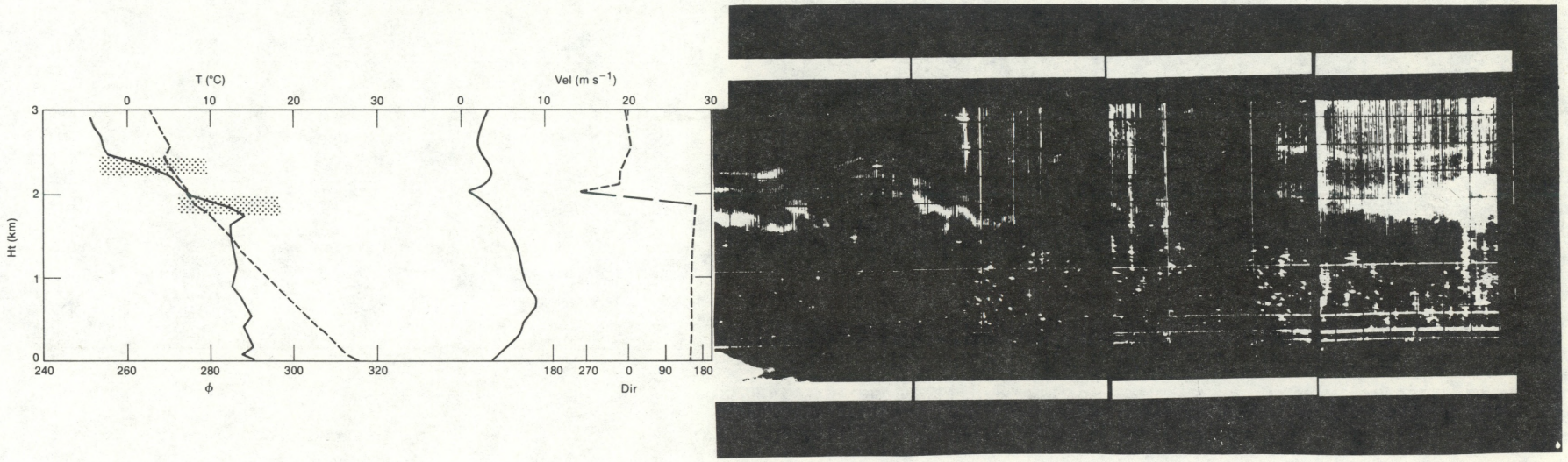

Figure 6. Record from 1522 - 1552 MST on 6 August 1974. Raob release 1535 MST.

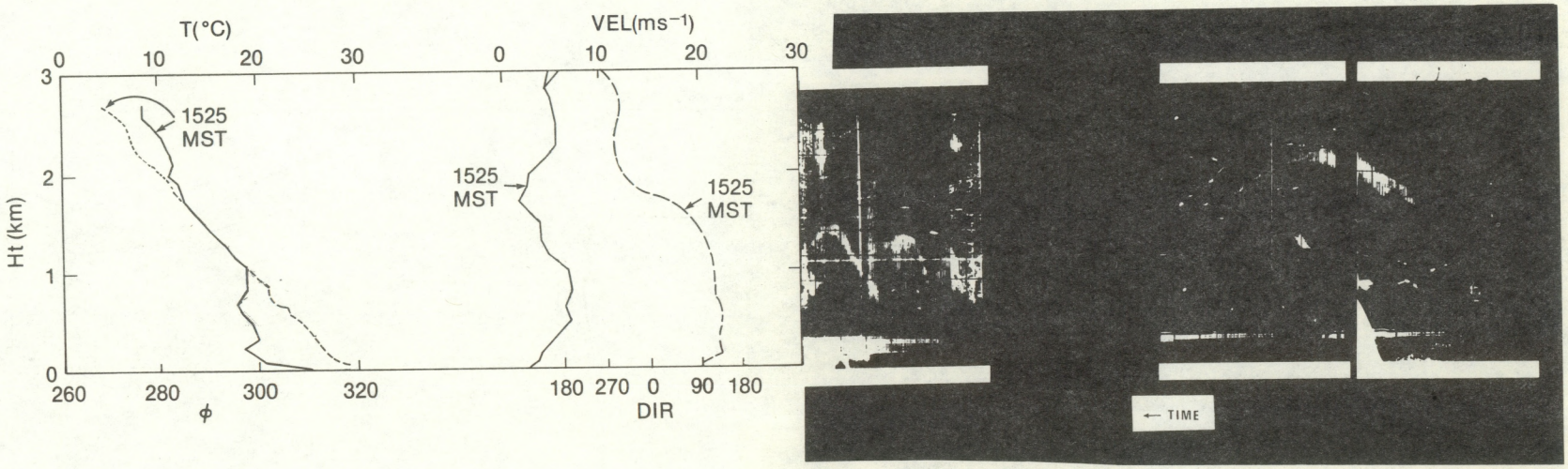

Figure 7. Record from 1508 - 1538 and 1550 - 1605 MST on 7 August 1974. No height scale change during "missing data" period. Raob release 1525 MST.

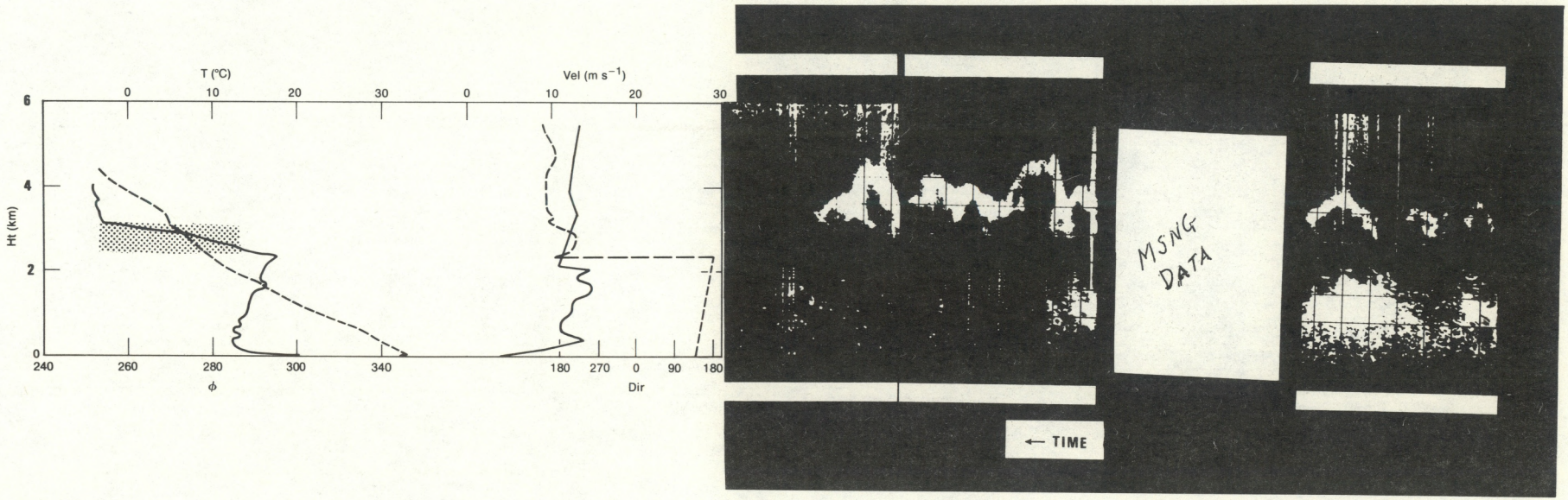

Figure 8. Records from 1602 - 1615 and 1646 - 1711 MST on 15 July 1974. Raob release 1525 MST.

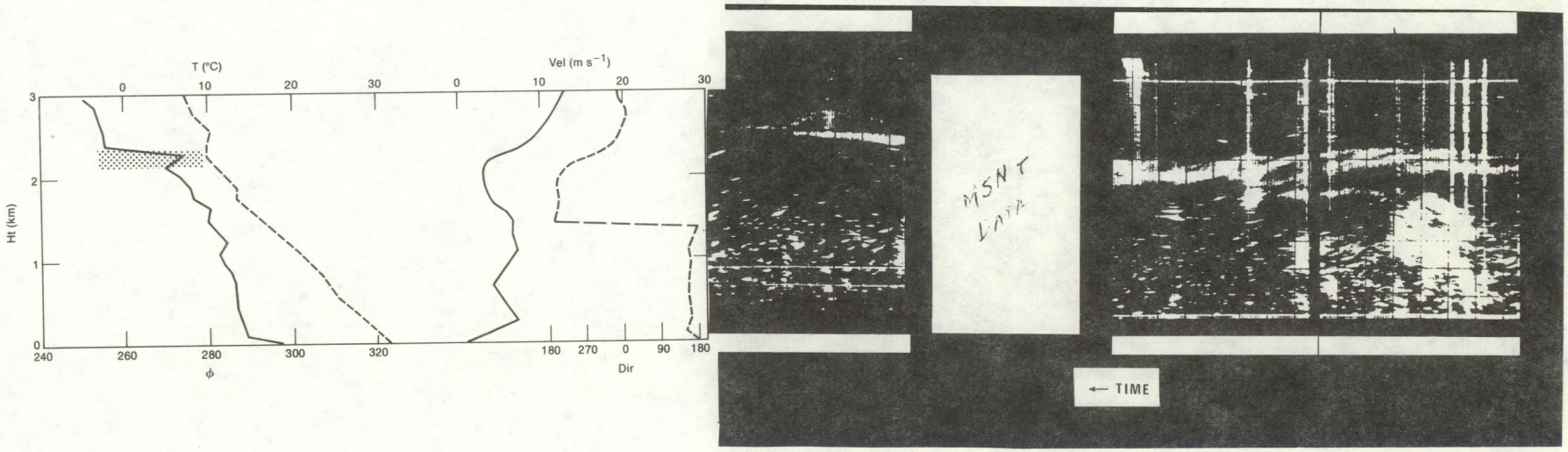

Figure 9. Record from 1222 - 1228 and 1242 - 1248 MST on 25 June 1974. Raob release 1530 MST.

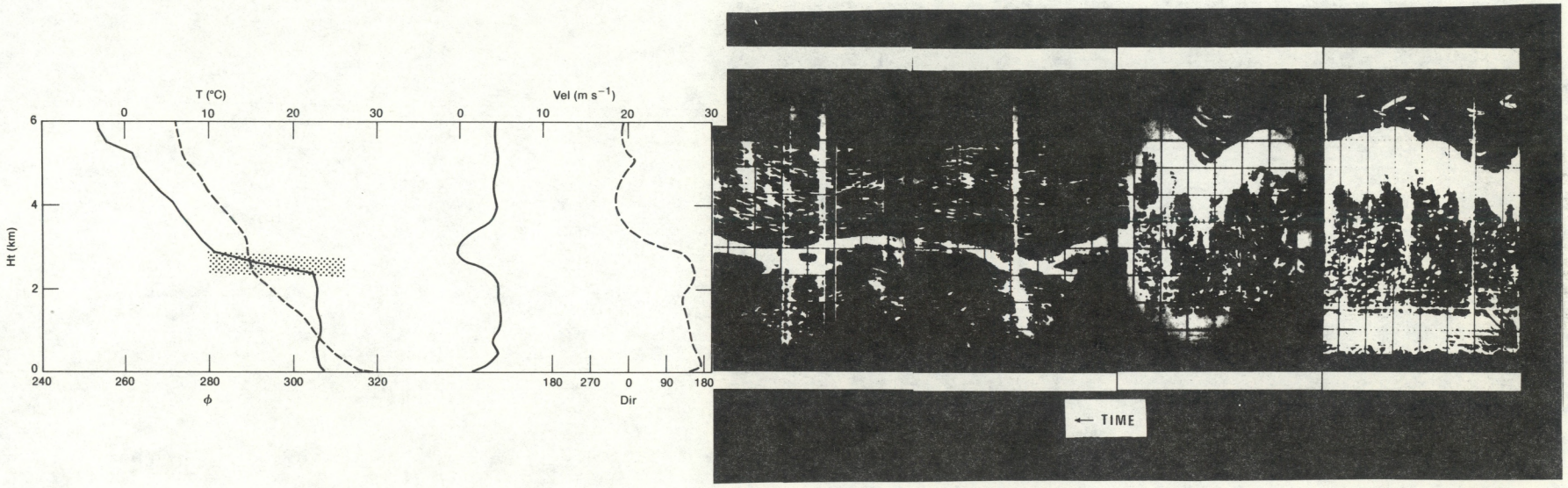

Figure 10. Record from 1212 - 1257 MST on 23 July 1974. Height scale changed midway through record. Raob release 1230 MST.

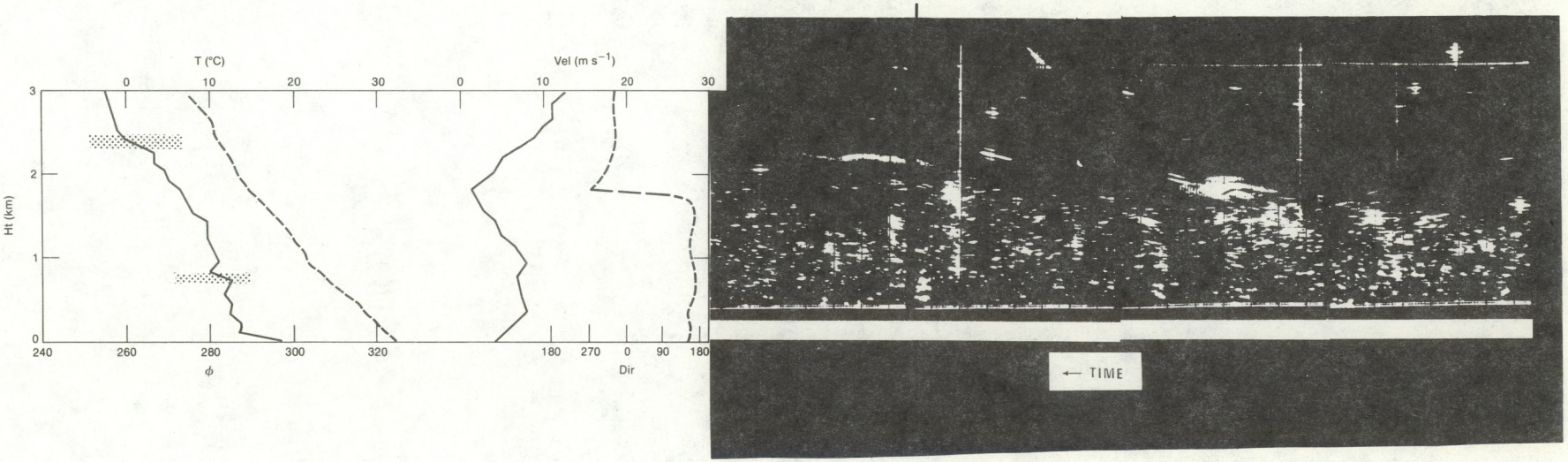

Figure 11. Record from 1522 - 1542 MST on 25 June 1974. Raob release 1530 MST.

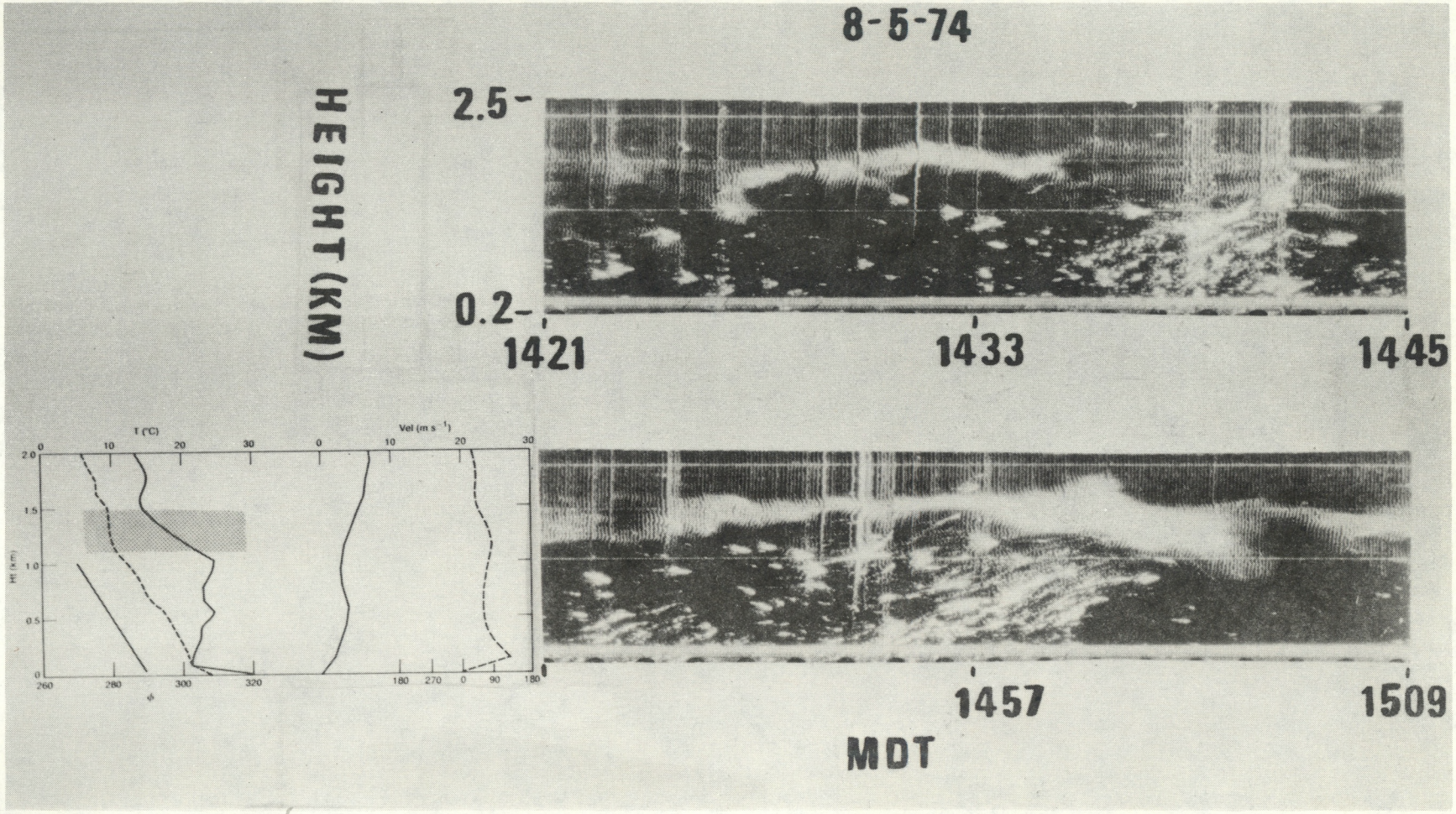

Figure 12. Record showing insects being swept up into convective dome. Raob release 1325 MDT (1225 MST).

case shown in Fig. 14 has been studied in detail previously, and an analysis of the Doppler velocity spectra through and above the inversion layer was carried out by Gossard et al. (1978) to obtain the profile of turbulent dissipation rate (ε) shown on the figure. Turbulent energy dissipation rate (ε) is calculated from the relation

$$\varepsilon = \delta^{-1}[\sigma_{11}^2/1.35\ A(1 - \gamma^2/15)]^{3/2} \qquad (3)$$

where $\delta = a$, $\gamma^2 = 1-(b/a)^2$ for $b/a < 1$

$\delta = b$, $\gamma^2 = 4[1-(a/b)^2]$ for $a/b < 1$.

The quantities a and b are the (Gaussian) beamsize and range cell size respectively, and σ_{11}^2 is the variance of the longitudinal velocity component within the pulse volume obtained from the observed width of the Doppler velocity spectrum. Using this expression for ε, the height gradient of refractive index within elevated layers can be measured with a Doppler radar as shown in Appendix B.

In this report we emphasize the enhanced backscatter from the elevate layer in Fig. 14. The radar obviously does an excellent job of detecting and monitoring the height of this type of atmospheric layer because of the large contrast in temperature and humidity across the layer that leads to a correspondingly large gradient in radio refractive index, ϕ. The synoptic situation for this event is shown in Fig. 15.

Figure 16 shows an event similar to that in Fig. 13 with prominent buoyancy waves on the inversion layer. The synoptic situation is shown in Fig. 17, and the similarity of the two cases is striking. The wave event is presently the subject of case studies, but for present purposes we emphasize the distribution of C_ϕ^2 across the inversion layer and the relation of the radar backscatter to the gradient structure. (The horizontal streaks are ground clutter and the occasional vertical streaks are probably birds in the beam.)

This case was also recorded on an acoustic sounder (SODAR) and the record for the interval from 0630 - 0740 MST (0730-0840 MDT) is shown in Fig. 18. The wave event is clearly recorded in the C_T^2 structure seen by the SODAR as well as the C_ϕ^2 structure observed by the radar. From the SODAR record it is possible to

calculate C_T^2 and from the radar record C_ϕ^2 can be calculated. It is readily shown (Gossard, 1978) that

$$C_\phi^2 = a^2 C_T^2 + b^2 C_e^2 - 2ab C_{Te}^2 . \qquad (4)$$

In Eq. (1)

$$a = \frac{7.76 \times 10^4}{\theta^2} + 7.46 \times 10^5 \frac{e_p}{\theta^3} , \quad b = \frac{3.73 \times 10^5}{\theta^2}$$

where θ is potential temperature and e_p potential vapor pressure. For the temperature and humidity at the time this case was recorded, $a \simeq 1.2$, $b \simeq 4.6$. C_{Te}^2 depends on the cross-covariance of temperature and humidity (Gossard, 1960).

From the acoustic and radar observations C_T^2 and C_ϕ^2 can be calculated. They are shown in Fig. 19 for "typical" profiles through the records of Figs. 15 and 17. Note that such "typical" profiles differ significantly from the average profiles as shown by the solid curve of C_T^2 superimposed on the typical profile in Fig. 18.

From Eq. 4, C_e^2 can be deduced if the correlation between temperature and humidity is known. For the case of 18 September the gradients of temperature and humidity are large and of opposite sign within the inversion layer. Therefore, it seems reasonable to suppose that mixing will create perturbations that are strongly negatively correlated. Assuming a correlation of -1, C_e^2 can be calculated from the observed values of C_ϕ^2 and C_T^2. The results are shown with the C_T^2 values in the left frame of Fig. 18. This is possibly the first measurement of C_e^2 in the atmosphere.

These data provide convincing evidence that clear air radars are able to detect reliably the important frontal type of layer structure when there are substantial contrasts in temperature and humidity across the front.

Conclusions

The radar is a reliable detector of elevated refractive index layers. In fact it provides a better estimate of the height and persistency of such layers

than do balloon soundings. The persistency is especially important because it allows transient and random apparent layers to be rejected. The one-shot balloon sounding cannot provide persistency information.

Insects can be an important contaminant to the records and must be reliably identified and rejected in geographical areas such as the U.S. Midwest.

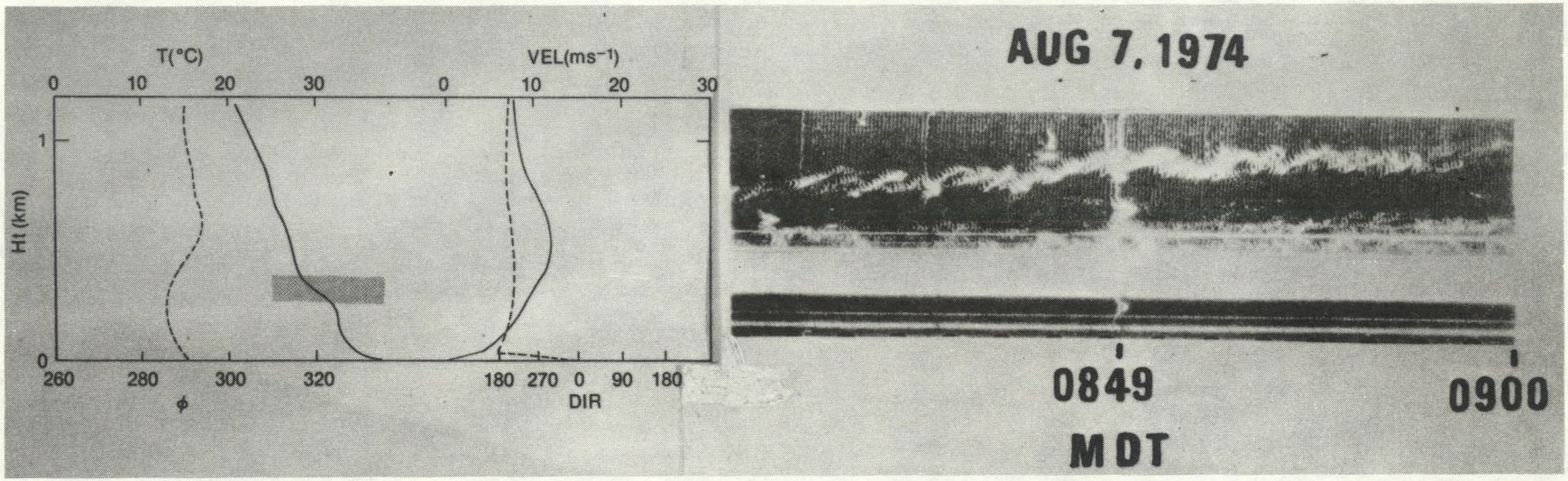

Figure 13. Raob was taken at 0725 MDT. I rate of change of layer height with time is taken into account, the layer seen on the radar record would agree very well with the layer seen in the balloon sounding.

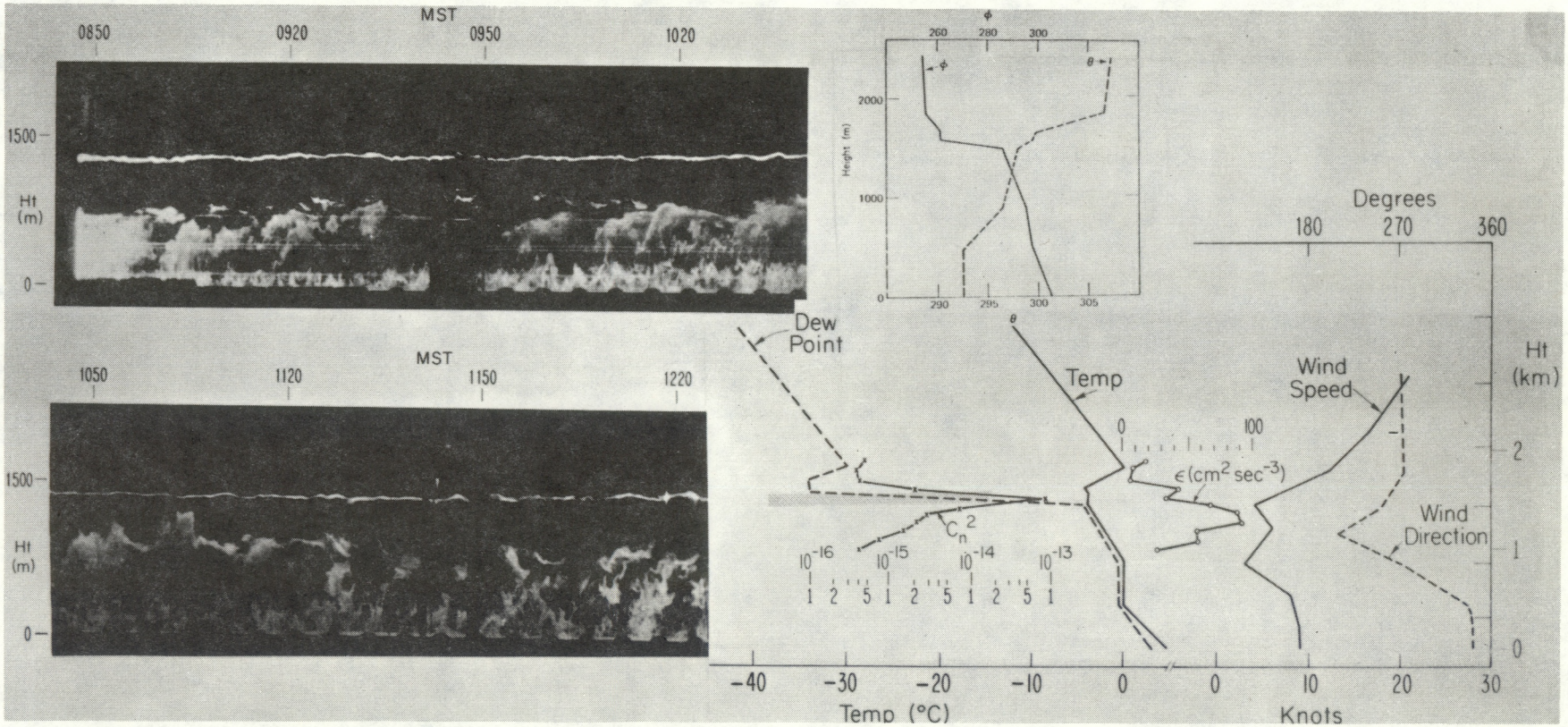

Figure 14. Record of 29 April 1976 from radar pointed vertically at Boulder, CO with 6 m height resolution showing frontal discontinuity at 1400 meter height. Sounding profiles are from raob taken at 0500 MST at Denver, CO.

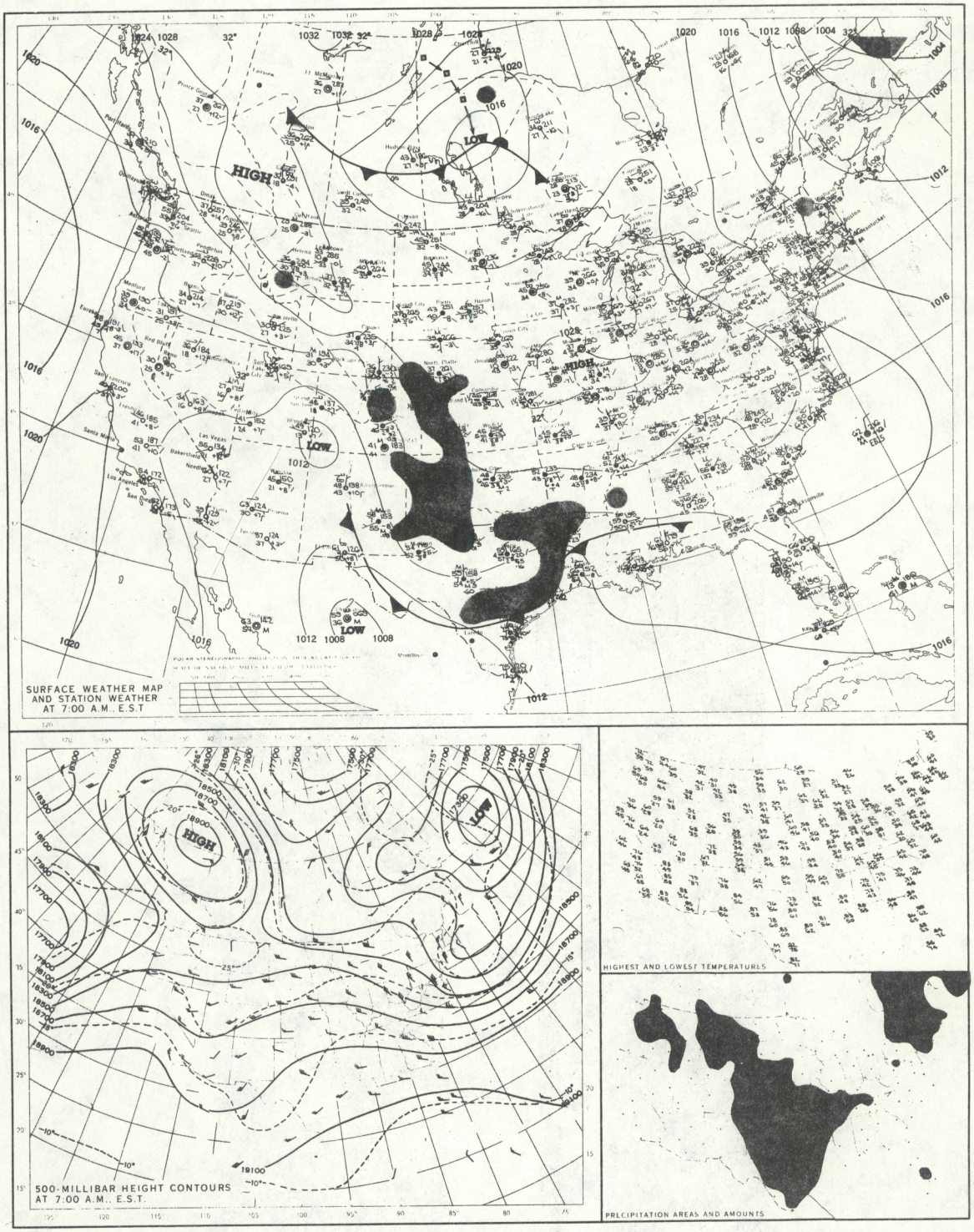

Figure 15. Surface weather map for 0500 MST.

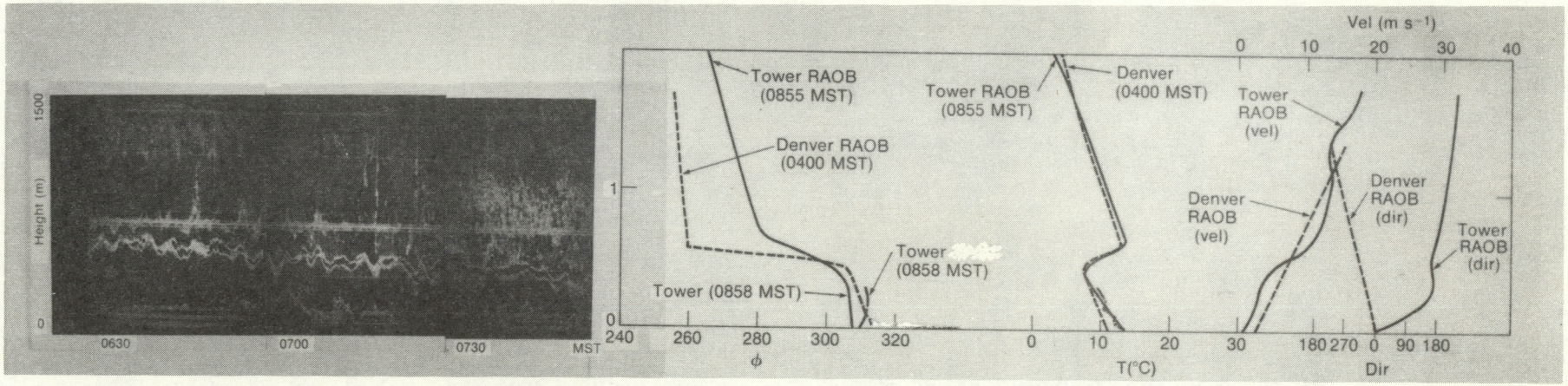

Figure 16. Record of 18 September 1978 from radar pointing vertically at Boulder, CO with 6 m height resolution showing frontal discontinuity with prominent buoyancy wave oscillations at a height of ∿600 m compared with two raobs: 0400 (release time) at Denver and 0858 MST at Boulder.

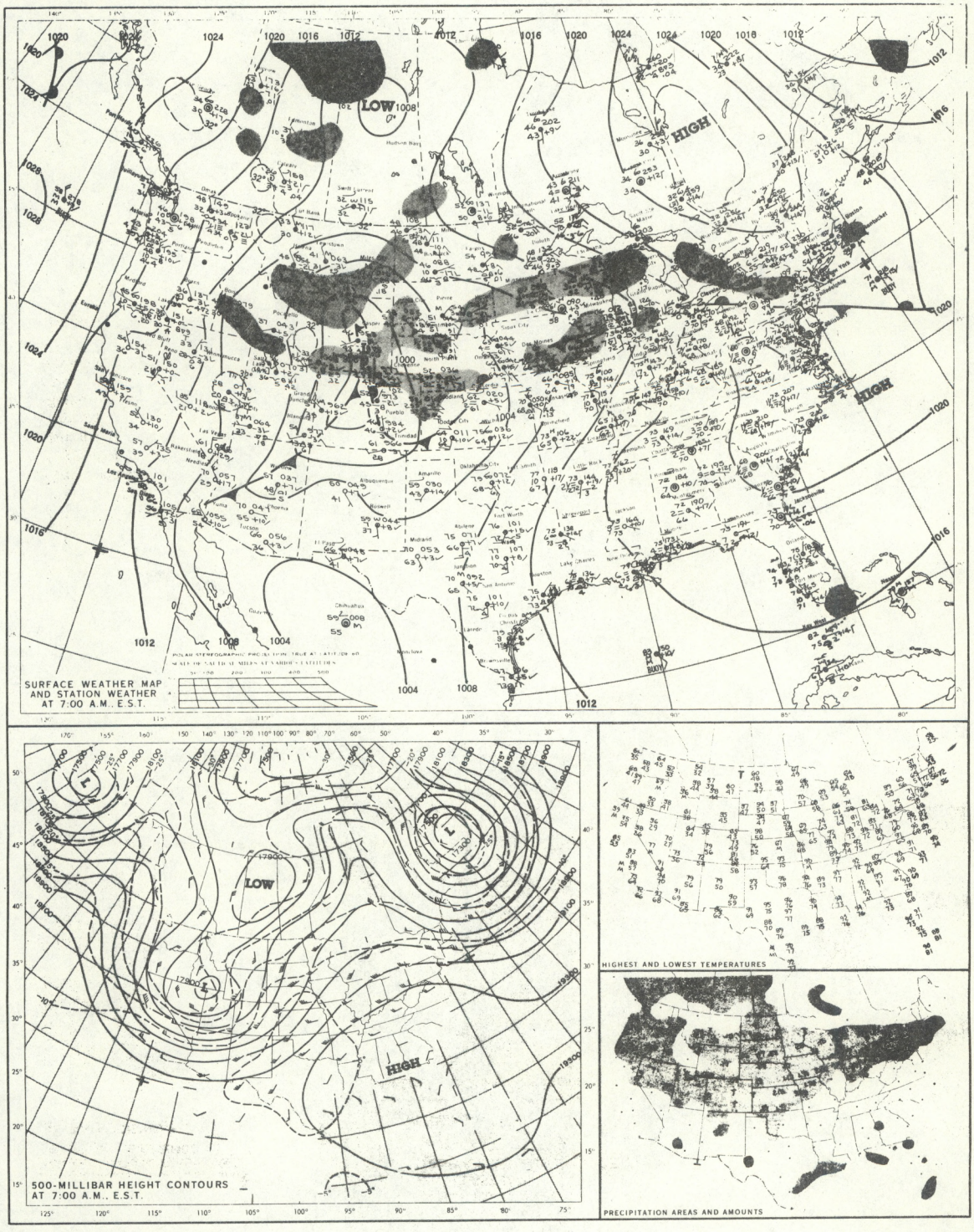

Figure 17. Surface weather map for 0500 MST, 18 September 1978.

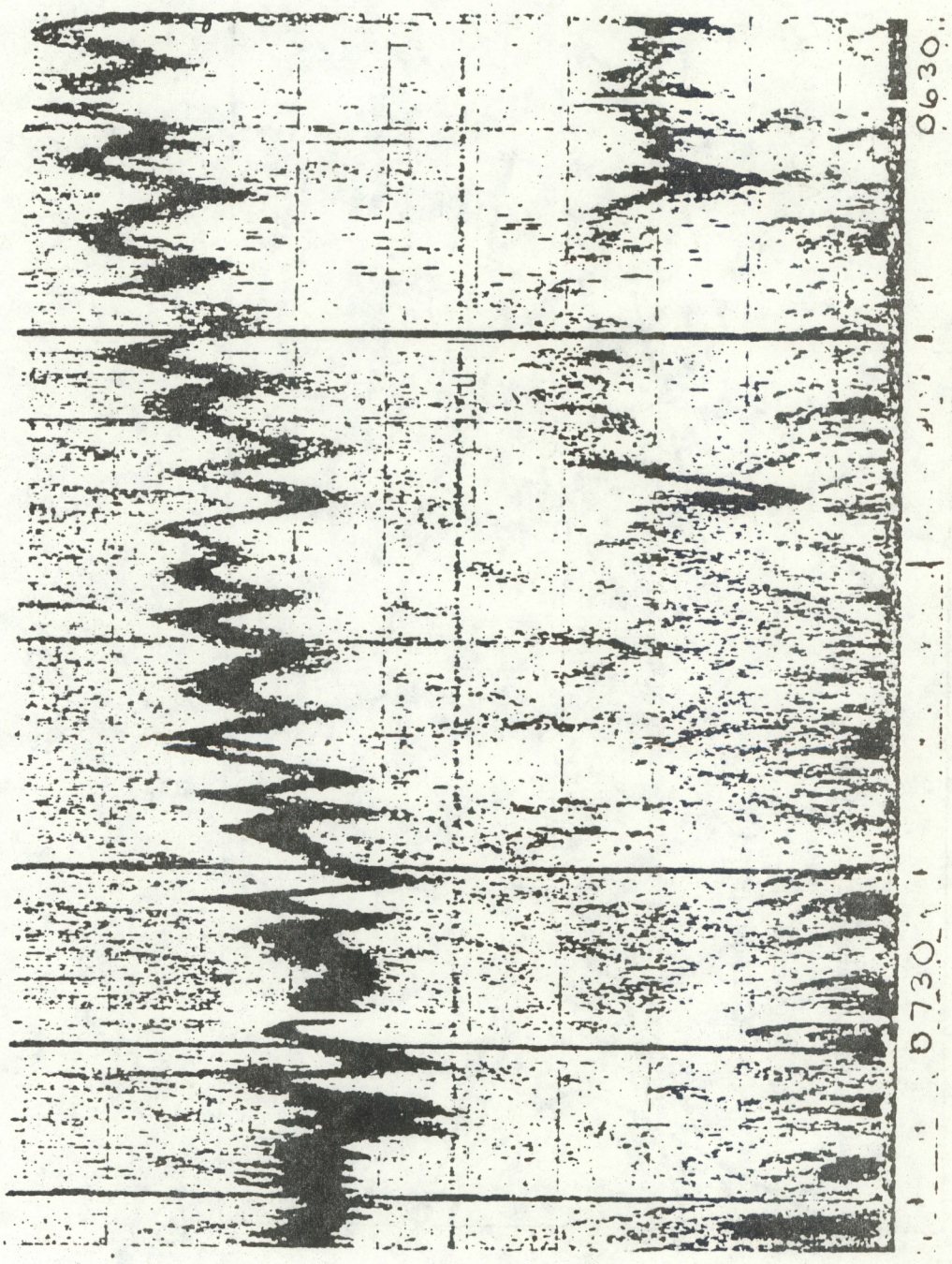

Figure 18. Acoustic sounder record corresponding to radar record of Fig. 16.

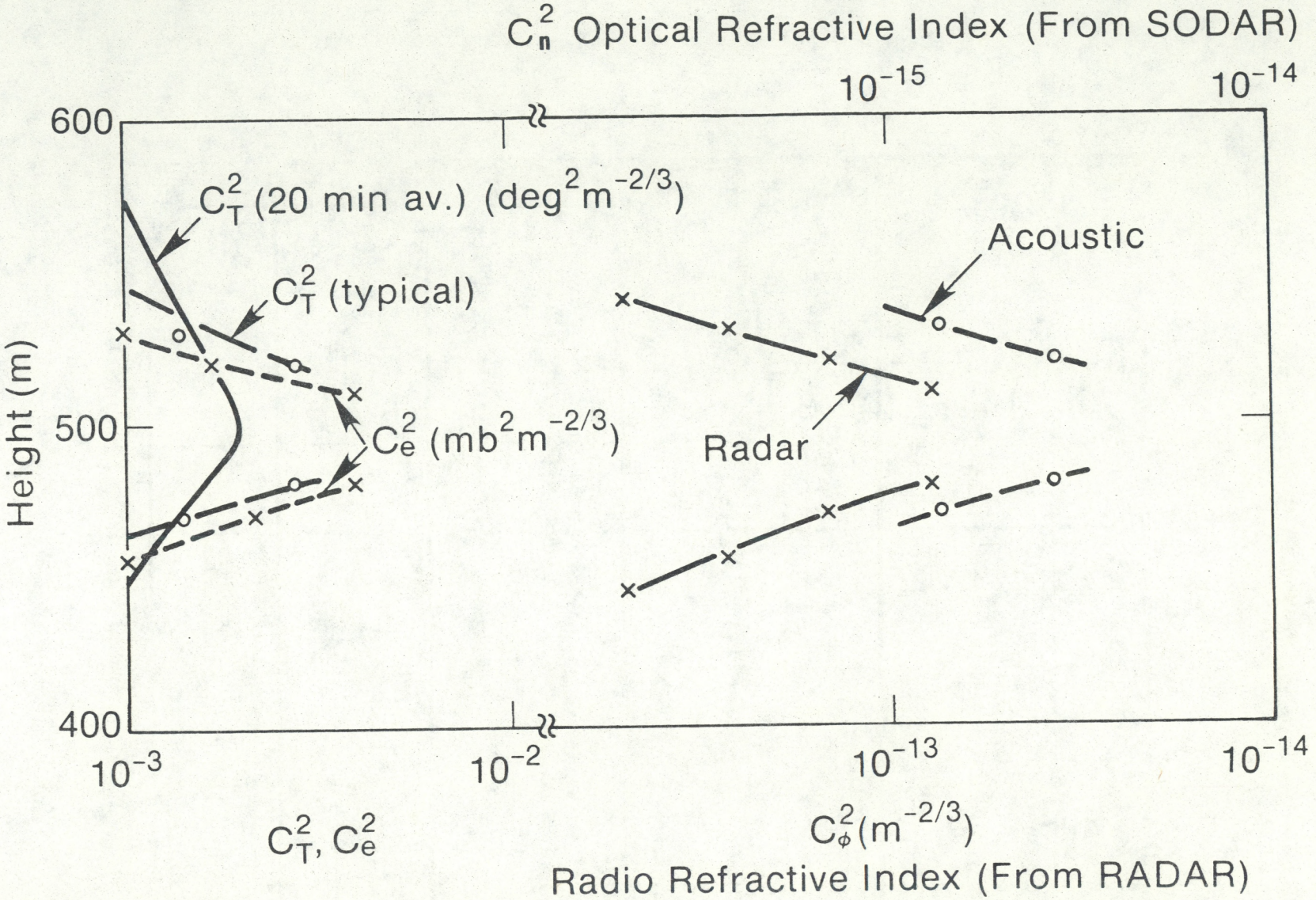

Figure 19. Height profiles of C_T^2 through the frontal interface of 18 September from acoustic sounder backscatter and profiles of C_ϕ^2 from FM-CW radar backscatter with profiles of optical C_n^2 calculated from C_T^2 and C_e^2 (structure constant for humidity) calculated from acoustic C_T^2 and radar C_ϕ^2.

Appendix A

For purposes of relating the refractive index to atmospheric physics, the most useful refractive index parameter is the potential refractive index ϕ which is more-or-less analogous to potential temperature and potential vapor pressure. In fact it is related to them as

$$\phi = \frac{77.6}{\theta}\left(1000 + \frac{4810 e_p}{\theta}\right) \qquad (1A)$$

where $\theta = T\,(1000/p)^{R/C_p}$ is potential temperature and $e_p = e\,(1000/p)$ is potential vapor pressure*. The temperature T is in Kelvin and the pressure p and the vapor pressure e are in millibars. Thus the potential quantities are the values of temperature, vapor pressure and refractive index characterizing an unsaturated air parcel if it were taken adiabatically from its level in the atmosphere to the 1000 mb level. These quantities are thus conserved during motions that are adiabatic, and they are useful because short-term (a few hours) atmospheric movements can usually be considered adiabatic.

Therefore it is useful to express the refractive index and refractive index structure constant in terms of ϕ and C_ϕ^2. Flavel and Lane (1962) have derived a relationship between ϕ and N as a function of pressure. This is done simply if we recall that

$$N = \frac{77.6}{T}\left(p + \frac{4810 e}{T}\right) \qquad (2A)$$

analogous to (1A). Then dividing (1A) and (2A)

$$\phi = N\, e^{0.714}(1 + 4810\, e/p\theta)/(1 + 4810\, e/pT). \qquad (3A)$$

Then, writing θ in terms of p and T, ϕ is expressed in terms of pressure, temperature and N. However, we are often given temperature and humidity as functions of <u>height</u>, so the Flavel and Lane expression is inappropriate.

* $R/C_p = 0.286$ where C_p is specific heat at constant pressure.

However writing the denominator of (8A) as TN/77.6 it is evident that

$$\phi = \left(\frac{1000}{p}\right)^{.714} \frac{77.6}{T}\left[p + \frac{4810e}{T}\left(\frac{1000}{p}\right)^{-.286}\right] .$$

Combining the hydrostatic equation,

$$dp = - \rho g \, dz \tag{4A}$$

with the equation of state,

$$\rho = \frac{P}{RT} \tag{5A}$$

where ρ is density, $g = 9.8$ m s^{-2} is gravitational acceleration and $R = 2.87 \times 10^{2}$ m^{2} s^{-1} deg^{-1} is the (dry) gas constant, we readily find that

$$d(\ell n \, p) = - \frac{g}{RT} \, dz \quad .$$

Therefore

$$\frac{1000}{p} = e^{(g/R\bar{T})(z-z_o)} \tag{6A}$$

where $\bar{T}$ is the value of T logarithmically averaged over the interval $z-z_o$ and z_o is the height at the 1000 mb level. Thus we define a function f(z) such that

$$\left(\frac{1000}{p}\right)^{-.286} \cong 1 - 0.286 \, (g/R\bar{T} \, (z-z_o) + \frac{1}{2}\left[0.286 \, (g/R\bar{T}) \, (z-z_o)\right]^2 \ldots \equiv f(z)$$

which converges quickly because $0.286 \frac{g}{RT} (z-z_o)$ is fairly small (i.e., < 0.29) for heights less than about 9 km. The next term in the expansion would contribute less than 0.4 of one percent at a height of 7.5 km.

Finally, assuming an exponential density distribution of scale height H, equation (5A) gives

$$\rho_o \, e^{-z/H} = (p/R\bar{T})$$

so

$$\frac{\partial p}{\partial z} = -\rho_o e^{-z/H} \, g \, dz = - (R\bar{T}/H) \, \rho_o \, e^{-z/H}$$

or

$$H = \frac{R\bar{T}}{g} \tag{7A}$$

is the scale height for the height interval $z-z_o$. Therefore, in terms of N, H(T) and height z

$$\phi = e^{0.714z/H} \, [N \, f(z) + (77.6)(0.286)(p/T)z/H] \, .$$

However from (5A) $P/T = \rho_o \, R \, e^{-z/H} \simeq 3.23 \, e^{-z/H}$ for soundings at Denver ($p \simeq 850$ mb) assuming the 1000 mb density $\rho_o \simeq 1.13 \times 10^{3}$ gr m^{-3}. (One millibar is one dyne $cm^{-2} = 10^{4}$ dynes m^{-2}). Therefore

$$\phi = e^{0.714z/H} [N \, f(z) + 71.95(z/H)e^{-z/H}] \tag{8A}$$

and

$$\frac{\partial \phi}{\partial z} = H^{-1} e^{0.714z/H} [f(z)H \, \frac{\partial N}{\partial z} + 71.95(1-z/H)e^{-z/H} - 0.286N(0.286z/H)] + 0.714H^{-1}\phi \tag{9A}$$

To develop an expression for $C_\phi^{\,2}$ in terms of $C_n^{\,2}$, note that the perturbation ϕ' is related to N' as

$$\phi' \equiv d\phi = \frac{\partial \phi}{\partial N} \, dN$$

so from eq. (2A)

$$\phi' = N' e^{0.814z/H} \, f(z) \, .$$

Therefore

$$C_\phi^2 = e^{1.428z/H} f^2(z) C_n^2 . \qquad (10A)$$

Appendix B.

A very general expression for C_ϕ^2 is

$$C_\phi^2 = a_o^2 \varepsilon^{-1/3} \varepsilon_\phi \tag{1B}$$

where ε is kinetic energy turbulent dissipation rate and ε_ϕ is rate of destruction of variance. The corresponding relation for temperature was given by Corrsin (1951). However, except under free convection which should not be relevant to elevated layers,

$$\varepsilon = -\overline{u'w'} \frac{\partial u}{\partial z} (1 - R_f) \tag{2B}$$

and

$$\varepsilon_\phi = - \overline{\phi'w'} \frac{\partial \phi}{\partial z} \tag{3B}$$

where primes denote perturbation quantities, w is vertical velocity and R_f is (flux) Richardson number. However, in terms of eddy coefficients

$$\overline{u'w'} = -K_m \partial u/\partial z \quad , \quad \overline{\phi'w'} = - K_\phi \partial \phi/\partial z \tag{4B}$$

so from (1B) (see e.g., Ottersten, 1969; Gossard, 1977)

$$C_\phi^2 = a_o^2 \varepsilon^{-1/3} K_\phi (\frac{\partial \phi}{\partial z})^2 .$$

If the mixing of momentum and the passive potential quantities is governed by similar physics, as is a good assumption in stable elevated layers, the Prandtl number is approximately unity so

$$K_\phi \simeq K_m = - \overline{u'w'} (\partial u/\partial z)^{-1} = \varepsilon/(\partial u/\partial z)^2 (1 - R_f) . \tag{5B}$$

Then using Eq. (3)

$$(\frac{\partial \phi}{\partial z})^2 = \frac{1.35 A}{a_o^2} \delta^{2/3} \frac{C_\phi^2 (\partial u/\partial z)^2}{\sigma_{11}^2} (1-R_f)(1-\gamma^2/15) . \tag{6B}$$

All quantities on the right-hand side of (6B) can be measured by Doppler radar except R_f. There is now considerable evidence that $R_f \simeq 0.25$ within elevated layers producing clear-air backscatter (Gossard et al., 1970, Bean et al., 1972). Therefore there appears to be little ambiguity in Eq. (6B). Panchev (page 245) gives $A = 1.35 \pm 0.06$ as the best value for A. Gurvich et al. (1967) conclude that $a_o^2 \simeq 2.8$, while Wyngaard et al. (1971) find $a_o^2 \simeq 3.2$. We suggest $A = 1.35$ and $a_o^2 = 3$ as probable best estimates.

REFERENCES

Bean, B. R., and E. J. Dutton, 1966: Radio Meteorology, Nat. Bur. Stand. Monogr. 92, 423 pp., U.S. Government Printing Office, Washington, DC.

Chadwick, R. B., K. P. Moran, R. G. Strauch, G. E. Morrison and W. C. Campbell, 1976: Microwave radar wind measurements in the clear air. Radio Sci., 11, 795-802.

Corrsin, S., 1951: On the spectrum of isotropic temperature fluctuations in isotropic turbulence. J. Appl. Phys., 22, 417-423.

Flavell and J. A. Lane, 1962: The application of potential refractive index in tropospheric wave propagation. J. Atmos. Terr. Phys., 24, 47-56.

Frisch, A. S., and S. F. Clifford, 1974: A study of convection capped by a stable layer using Doppler radar and acoustic echo sounders. J. Atmos. Sci., 31, 1622-1628.

Gossard, E. E., 1960: Power spectra of temperature, humidity, and refractive index from aircraft and tethered balloon measurements. IRE Trans. Antennas Propagat., AP-8, 186-201.

Gossard, E. E., 1979: The use of radar observations of C_n^2 vs. height to deduce height profiles of refractive index. NOAA Tech. Memo. ERL WPL-47, 52 p.

Gossard, E. E. and J. H. Richter, 1970: The shape of internal waves of finite amplitude from high-resolution radar sounding of the lower atmosphere, J. Atmos. Res., 27, 971-973.

Gossard, E. E., D. R. Jensen and J. H. Richter 1971: An analytical study of tropospheric structure as seen by high-resolution radar. J. Atmos. Sci., 28, 794-807.

Konrad, Thomas G., 1970: The dynamics of the convective process in clear air as seen by radar. J. Atmos. Sci., 27, 1138-1147.

Labitt, M., 1979: Some basic relations concerning the radar measurement of air turbulence, MIT, Lincoln Laboratory, ATC Working Paper No. 46WP-5001.

Ottersten, H. (1969: Atmospheric structure and radar backscattering in clear air. Radio Sci., 4, 1179-1193.

Panchev, S. (1971: Random Functions and Turbulence. Pergamon Press, 444 p.

Richter, Juergen H., Douglas R. Jensen, and V. Ray Noonkester, Thomas G. Konrad, Abraham Arnold, John R. Rowland, 1974: Clear air convection: A close look at its evolution and structure. Geophys. Res. Letts., 1, 173-176.

Richter, J.H. and E. E. Gossard, 1970: Lower tropospheric structure as seen by a high-resolution radar. NELC/TR 1718, 66 pp.

Richter, J. H., 1969: High resolution tropospheric radar sounding, Radio Sci., 4, 1260-1268.

Strauch, R. G., W. C. Campbell, R. B. Chadwick and K. P. Moran, 1976: Microwave FM-CW Doppler radar for boundary layer probing. Geophys. Res. Letts., 3, No. 1.

Wyngaard, J. C., Y. Izumi and S. A. Collins, Jr. 1971: Behavior of the refractive-index-structure parameter near the ground. J. Opt. Soc. Amer., 61, 1646-1650.